Direct Observation of Chiral Magnon Splitting in Altermagnetic CrSb

H.J. Elmers,[1,*] Y. Lytvynenko,[1,2] C. Fawaz,[3] T. Lacmann,[4] S. V. Chernov,[5] O. Tkach,[1] H. Agarwal,[1] J. O. Schunck,[6,7] D. Kutnyakhov,[5] J. Dilling,[8,9] L. Bruckmeier,[8,9] M. Merz,[3] N. Maraytta,[3] L. Filsinger,[3] M. Scholz,[5] M. Hoesch,[5] K. Rossnagel,[8,9] A. Haghighirad,[3] M. Jourdan,[1] J. Demsar,[1] O. Fedchenko,[10] G. Schönhense,[1] M. Beye,[11] and M. Le Tacon[3]

[1] *Institut für Physik, Johannes Gutenberg-Universität, Staudingerweg 7, D-55128 Mainz, Germany*
[2] *V. G. Baryakhtar Institute of Magnetism of the NAS of Ukraine, 03142 Kyiv, Ukraine*
[3] *Institute for Quantum Materials and Technologies, Karlsruhe Institute of Technology, 76021 Karlsruhe, Germany*
[4] *Laboratory for Quantum Magnetism, Institute of Physics, École Polytechnique Fédérale de Lausanne (EPFL), 1015 Lausanne, Switzerland*
[5] *Deutsches Elektronen-Synchrotron DESY, 22607 Hamburg, Germany*
[6] *Department of Physics, Stockholm University, AlbaNova University Center, 106 91 Stockholm, Sweden*
[7] *Wallenberg Initiative Materials Science for Sustainability, Department of Physics, Stockholm University, 106 91 Stockholm, Sweden*
[8] *Institut für Experimentelle und Angewandte Physik, Christian-Albrechts-Universität zu Kiel, 24098 Kiel, Germany*
[9] *Ruprecht Haensel Laboratory, Deutsches Elektronen-Synchrotron DESY, 22607 Hamburg, Germany*
[10] *Physikalisches Institut, Goethe Universität Frankfurt, 60438 Frankfurt am Main, Germany*
[11] *Stockholm University, Roslagstullsbacken 21 Stockholm, Sweden*

(Dated: May 23, 2026)

I. ANGLE-RESOLVED PHOTOEMISSION SPECTROSCOPY

We mapped the band structure of CrSb in three-dimensional momentum space to confirm the altermagnetic electronic band splitting using soft X-ray angle-resolved photoemission spectroscopy (ARPES). Using higher photon energies provides more bulk-like information and avoids changes to the electronic structure caused by the surface. Figure 1 shows the electronic band dispersion in CrSb, measured with soft X-ray excitation at energies of $h\nu = 715$ eV and $h\nu = 665$ eV. Assuming a free-electron final state model, these photon energies result in perpendicular electron momenta at $k_z = 12.05 G_{001}$ and $k_z = 11.45 G_{001}$, where G_{001} refers to the reciprocal lattice vector along the Γ-A direction [see Fig. 1b]. As the k_z-values are close to the high-symmetry points Γ and A in the repeated Brillouin zone scheme, the band dispersions are probed approximately along the indicated high symmetry directions.

Figure 1c shows a cross-section of the three-dimensional Fermi surface in the K-Γ-M plane. The sixfold symmetric pattern reflects the six-fold hexagonal symmetry perpendicular to the *c*-axis. A constant energy cut at a higher binding energy of $E_B = 300$ meV (Fig. 1d) shows an increase in the size of the pattern, indicating the hole-like character of the electronic states. When $E_B = 300$ meV, the difference in band dispersion between the paths along Γ-M and Γ-K is most pronounced.

The exchange-split, hole-like bands, α and β, which run close to the M-Γ-M direction, as shown in Fig. 1e, have an almost constant energy splitting of 0.7 eV in agreement with previous results [1]. Additional bands γ and δ can also be identified. The section along the K-Γ-K direction (Fig. 1f) shows two separate bands ϵ and ζ. The band dispersions in the H-A-L plane display only a single band along the L-A-L and H-A-H directions (Fig. 1i,j).

Varying the photon energy between $h\nu = 715$ eV and $h\nu = 665$ eV and exploiting crystal symmetries results in the four-dimensional array, $I(E_B, k_x, k_y, k_z)$, which allows the complete Brillouin zone to be mapped. The perspective view of the three-dimensional Fermi surface (Fig. 1k) shows a central cylinder with the six-fold protrusions close to the K-Γ-M and H-A-L high-symmetry planes. The dispersion along the k_z direction is visualised in the cut-out drawings of the Fermi surface and the constant energy surface at $E_B = 0.3$ eV (see Fig. 1l,m).

II. EVALUATION STEPS

Figure 2 illustrates the steps of data evaluation. The measured photoemission intensities, $I^{+/-}(E_F, k_x, k_y,$ for circularly right (+) and left (-) polarized X-rays are symmetrized with respect to the $(k_x, k_y = 0)$ line. This sym-

* elmers@uni-mainz.de

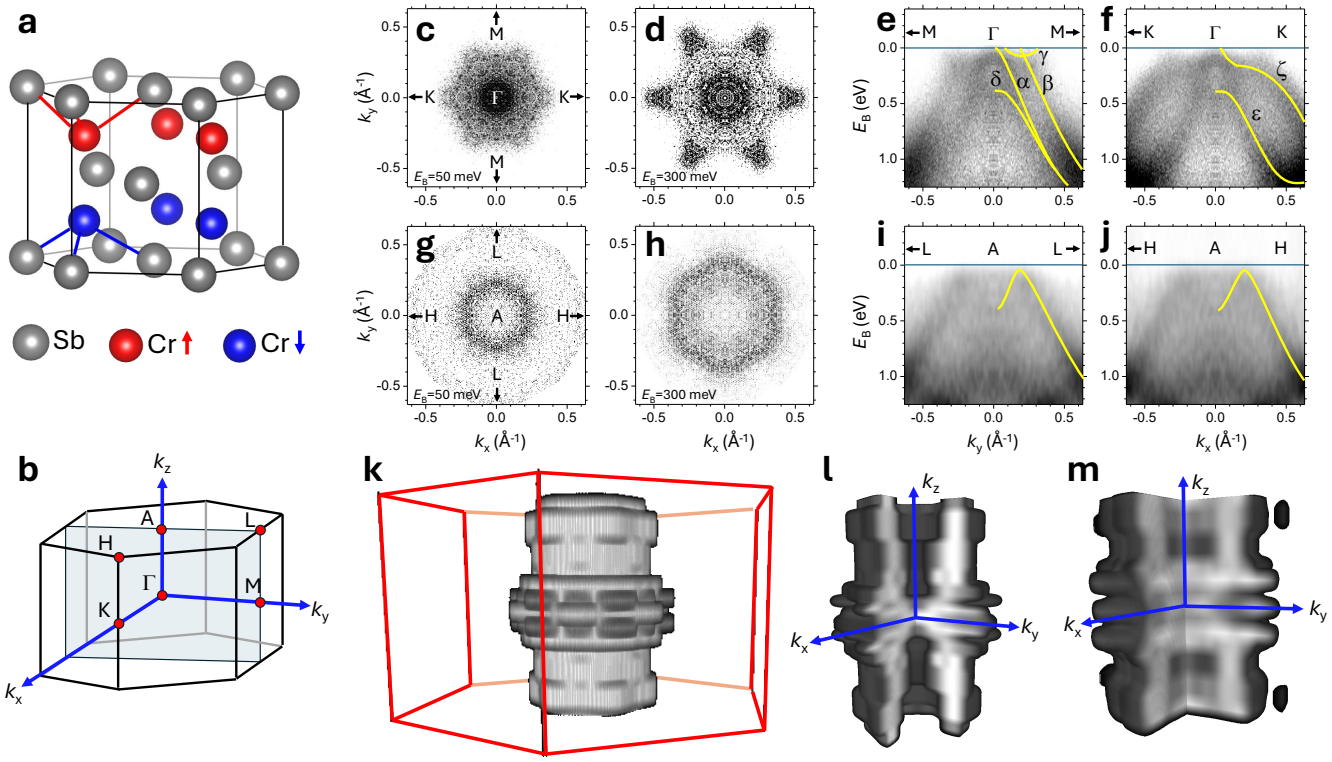

FIG. 1. Band mapping of CrSb(001) using soft X-ray ARPES. a. The hexagonal crystal structure of CrSb illustrating the staggered altermagnetic orientation of Cr moments. The alternating Cr magnetic moments are aligned parallel to the c-axis and are separated by Sb planes. b. The reciprocal unit cell indicates the high symmetry points. The scattering plane of the incident X-rays is aligned parallel to the grey-shaded A-Γ-M plane. c. Photoemission intensity map at a constant binding energy of $E_B = 30$ meV measured with a photon energy of $h\nu = 715$ eV. d. Similar data from the same data set at $E_B = 300$ meV. The corresponding perpendicular momentum at this photon energy is $k_z = 12.05 G_{001}$ and the K-Γ-M plane is probed. e. and f. Constant momentum sections $I(E_B, k_x = 0, k_y)$ and $I(E_B, k_x, k_y = 0)$ showing the band dispersion along the Γ-M and Γ-K directions. g.-j. Similar data for excitation with a photon energy of $h\nu = 665$ eV, corresponding to the perpendicular momentum $k_z = 11.55 G_{001}$ and the probed H-A-L plane. k. Three-dimensional representation of the outer Fermi surface sheet. l. A cut-out drawing of the Fermi surface showing cuts in the k_z-k_x and k_z-k_y planes, drawn on the same scale. m. Similar cut-out drawing of a constant energy surface at $E_B = 300$ meV.

metrisation step avoids any asymmetry contribution due to linear dichroism, which may appear because the angle of incidence of the x-ray light is $\theta = 22.5°$ and therefore the p and s components of the circularly polarized light are not equivalent. This component is in fact quite small [2].

The first step is to evaluate the sum and difference of the intensity maps measured for the two opposite circular X-ray polarizations. The difference divided by the sum gives the asymmetry $A^*(E_B, k_x, k_y)$ as shown in Fig. 2(a) for $E_B = E_F$. To better illustrate positive and negative asymmetries, we plot the asymmetry maps on a red (positive)/blue(negative) colour scale. The maximum asymmetries are approximately 0.5.

To separate the CDAD and MCDAD contributions to the measured asymmetry, the opposite symmetry relations are exploited. The CDAD asymmetry is strictly antisymmetric with respect to the $(k_x = 0, k_y)$ line (i.e., the plane spanned by the x-ray reflection plane coincident with the crystal mirror plane). Consequently, the CDAD asymmetry is given by

$$A_{\mathrm{CDAD}}(k_x, k_y) = (1/2)[A^*(k_x, k_y) - A^*(-k_x, k_y)] \tag{1}$$

[Fig. 2(b)] for any binding energy E_B. Fig. 2(b) shows the result for $E_B = E_F$.

Instead, the MCDAD asymmetry, given by

$$A_{\mathrm{MCDAD}}(k_x, k_y) = (1/2)[A^*(k_x, k_y) + A^*(-k_x, k_y)]. \tag{2}$$

A_{MCDAD} is symmetric with respect to the $(k_x = 0, k_y)$ line [Fig. 2(c)]. The maximum MCDAD asymmetries are 0.25

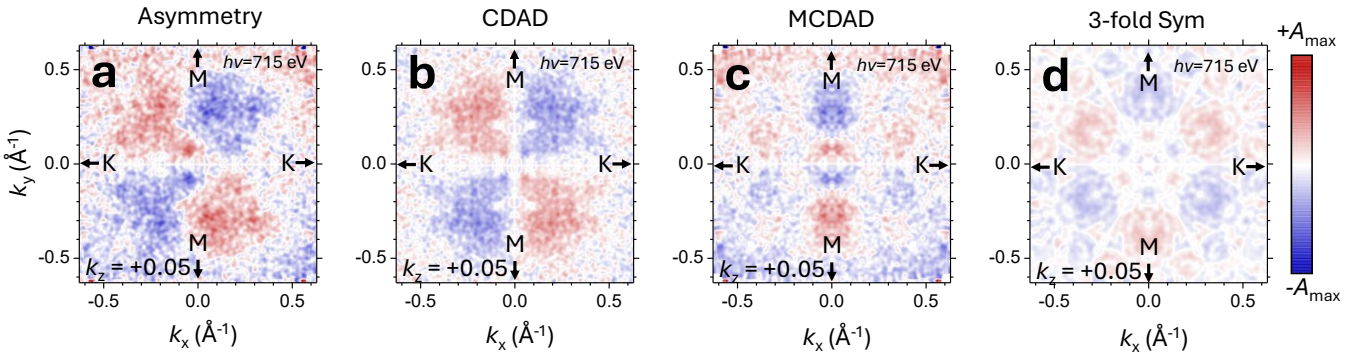

FIG. 2. (a) Asymmetry, $A^* = I_{\rm dif}(E_F, k_x, k_y)/I_{\rm sum}(E_F, k_x, k_y)$ image, calculated from the difference image, $I_{\rm dif}(E_F, k_x, k_y) = I^+(E_F, k_x, k_y) - I^-(E_F, k_x, k_y)$ and the sum image $I_{\rm sum}(E_F, k_x, k_y) = I^+(E_F, k_x, k_y) + I^-(E_F, k_x, k_y)$. The photoemission intensity $I^{+/-}(E_F, k_x, k_y$ was measured for circularly right (+) and left(-) X-ray light with photon energy of 715 eV. X-ray light shines from the top with projected beam parallel to the k_y-axis. The color scale for (a) and (b) is $A_{\rm max} = 0.5$. (b) Circular dichroism in the angular distribution calculated by: $A_{\rm CDAD} = A^*(E_F, k_x, k_y) - A^*(E_F, -k_x, k_y)$. (c) Magnetic circular dichroism in the angular distribution calculated by: $A_{\rm MCDAD} = A^*(E_F, k_x, k_y) + A^*(E_F, -k_x, k_y)$. (d) Three-fold symmetrisation of $A_{\rm MCDAD}$. The color scale for (c) and (d) is $A_{\rm max} = 0.25$.

appearing along the central symmetry line ($k_x = 0, k_y$). Additional data shown in the main text are evaluated in a similar way.

III. X-RAY ABSORPTION SPECTROSCOPY

X-ray absorption spectroscopy (XAS) was performed prior to the RIXS measurements and is based on the total fluorescence yield method. Fig. 3 shows the XAS spectrum for circular right polarized X-ray light. We did not observe any dichroism signal in agreement with the observation reported in Ref. 3. The vertical dashed line indicates the selected photon energy for RIXS.

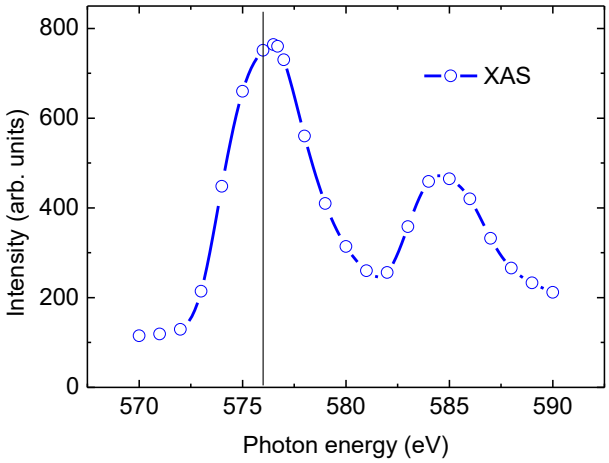

FIG. 3. X-ray absorption spectrum from total fluorescence yield measurements using incident X-rays with circular-right (CR) polarisation with an incidence angle of 22.5 degrees, measured at the same position as for the RIXS measurements. The vertical dashed line indicates the selected photon energy (576 eV) for RIXS.

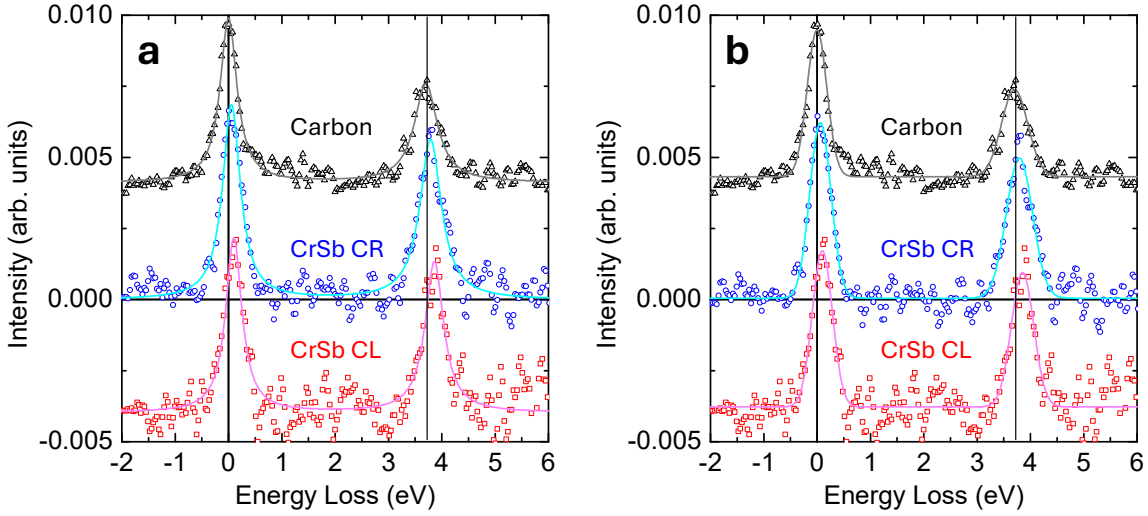

FIG. 4. a. PAX-RIXS spectra at the Cr L-edge maximum. Reference PAX-RIXS spectrum (black), measured for a polycrystalline carbon sample and shifted by +0.004 for better visibility. The fits using a Lorentzian function is shown as a full line. This reference spectrum establishes the zero energy loss point for purely elastic scattering. The PAX-RIXS spectra of CrSb (blue/red) were measured using the same geometry for circularly polarised excitation (blue for right and red for left, the latter spectrum shifted by −0.004 for better visibility). Fits using Lorentzian functions are shown as full lines. The shift of the intensity maxima to increasing energy loss is caused by the inelastic scattering process. b. The same experimental data, fitted using Gaussian functions. The fit parameters for these functions are provided in Table 2.

IV. PEAK FITTING

Figure 4 shows the reference spectrum (black), obtained by elastic scattering from a polycrystalline carbon sample positioned next to the CrSb sample in the same experimental run. This spectrum corresponds to a conventional XPS spectrum of Au. Fitting the two peaks with Gaussian functions determines the zero energy loss locations on the abscissa for the two Au $4f$ conversion lines.

The spectra of circularly polarised X-ray light scattered at the CrSb sample (shown in blue and red in Fig. 4) show significant shifts of the peak maxima to larger energy losses. These shifts are larger for circular left polarisation than for circular right polarisation. This observation indicates that the inelastic scattering is dominated by energy losses within a narrow energy range. The significant polarisation dependence of the peak shifts excludes phonon-mediated scattering and supports the interpretation as magnon scattering.

Sample	E_1^0 (meV)	σ_1^E (meV)	w_1 (meV)	σ_1^w (meV)	E_2^0 (meV)	σ_2^E (meV)	w_2 (meV)	σ_2^w (meV)
Carbon	0	5	370	10	3704	10	493	21
CrSb-CR	61	6	396	12	3793	8	493	17
CrSb-CL	97	10	378	21	3852	12	421	26

TABLE I. Results of least squares fitting of two Gaussian functions (Eq. 3) to the experimental data. The centers of the two peaks are E_1^0 and E_2^0. The full widths of the peaks at half height are denoted as ω_1 and ω_2. The statistical errors are given as the standard deviations σ_i^E and σ_i^ω, with $i = 1, 2$. The peak areas for circular right and left polarisation are approximately the same.

The observed peaks were fitted with two Gaussian functions:

$$I(E) = \frac{A_i}{\omega_i \sqrt{\pi/2}} e^{-2(\frac{E-E_i}{\omega_i})^2} + I_0, \tag{3}$$

where E_i^0 denotes the energy of the intensity maximum ($i = 1, 2$), A_i is the peak area, ω_i is the peak width, and I_0 describes the energy-independent background intensity. The relevant fit parameters are given in Table I.

[1] J. Ding, Z. Jiang, X. Chen, Z. Tao, Z. Liu, T. Li, J. Liu, J. Sun, J. Cheng, J. Liu, Y. Yang, R. Zhang, L. Deng, W. Jing, Y. Huang, Y. Shi, M. Ye, S. Qiao, Y. Wang, Y. Guo, D. Feng, and D. Shen, Large band splitting in g -wave altermagnet crsb, Physical Review Letters **133**, 206401 (2024).

[2] H. Elmers, O. Tkach, Y. Lytvynenko, P. Yogi, M. Schmitt, D. Biswas, J. Liu, S. Chernov, Q. Nguyen, M. Hoesch, D. Kutnyakhov, N. Wind, L. Wenthaus, M. Scholz, K. Rossnagel, A. Gloskovskii, C. Schlueter, A. Winkelmann, A.-A. Haghighirad, T.-L. Lee, M. Sing, R. Claessen, M. Le Tacon, J. Demsar, G. Schönhense, and O. Fedchenko, Chirality in the Kagome Metal CsV3Sb5, Physical Review Letters **134**, 096401 (2025).

[3] N. Biniskos, M. dos Santos Dias, S. Agrestini, D. Sviták, K.-J. Zhou, J. Pospíšil, and P. Čermák, Systematic mapping of altermagnetic magnons by resonant inelastic x-ray circular dichroism, Nature Communications **16**, 10.1038/s41467-025-64322-0 (2025).